

Reality-based Estimation of Needle and Soft-tissue Interaction for Accurate Haptic Feedback in Prostate Brachytherapy Simulation*

James T. Hing[†], Ari. D. Brooks^{††}(MD), Jaydev P. Desai^{†a} (PhD)

[†]*Program for Robotics, Intelligent Sensing, and Mechatronics (PRISM) Laboratory, Drexel University, Philadelphia, PA*

^{††}*Drexel University College of Medicine, Philadelphia, PA*

Abstract – Prostate Brachytherapy is the implantation of radioactive seeds into the prostate as a treatment for prostate cancer. The success rate of the procedure is directly related to the physician’s level of experience. In addition, minor deviations in seed alignment caused by gland compression/retraction, gland edema (swelling) and needle deflections can create significant areas of over or under dosage to the gland and/or injury to surrounding nerves and organs, leading to increased morbidity. Therefore, reductions in brachytherapy complication rates will be dependent on improving the tools physicians use for training to improve the accuracy of needle guidance and deployment of ‘seeds’ within the prostate gland. Through our novel approach of using two C-ARM fluoroscopes, we propose a reality-based approach for estimating needle and soft tissue interaction for the purpose of eventually developing an accurate seed placement training simulator with haptic feedback for prostate brachytherapy. By recording implanted fiducial movement and needle-soft tissue interaction forces, we can: extract the local effective modulus during puncture events, quantify tissue deformation, obtain an approximate cutting force, and build a finite element model to provide accurate haptic feedback in the training simulator for needle insertion tasks.

Index Terms – Surgical Simulation, Soft-tissue Modeling, Prostate Brachytherapy, Local Effective Modulus.

* This work was supported in part by National Science Foundation CAREER award IIS 0133471 and NSF ITR award 0312709.

Mr. James Hing is a graduate student in the PRISM laboratory (e-mail: jth23@coe.drexel.edu).

Dr. Ari D. Brooks is a General Surgeon specializing in Surgical Oncology at Drexel University College of Medicine (email: Ari.Brooks@DrexelMed.edu).

Dr. Jaydev P. Desai is the Director of the PRISM Laboratory, Drexel University, Philadelphia, PA 19104, USA (corresponding author, phone: 215-895-1738; fax: 215-895-1940; e-mail: desai@coe.drexel.edu).

^a Corresponding author.

I. INTRODUCTION

Prostate cancer is the most common cancer in men in the United States and it is the second leading cause of cancer deaths in men [1]. The prevalence is about 10 to 20 times the incidence because the vast majority of affected men will not die of prostate cancer. This identifies an important issue regarding the treatment of prostate cancer: the quality of life for what amounts to a normal remaining life span becomes extremely important [2]. Patients have three main choices for treatment of prostate cancer: surgical excision, radiation therapy, and expectant management/hormone therapy [3], and each approach is associated with acceptable long-term survival. The difference between these therapies lies in the associated outcomes of treatment, i.e. acute and chronic complications/side effects that can limit one's enjoyment of life and even lead to chronic conditions requiring medical intervention, medications, surgical procedures, hospitalizations, and even death [2]. Since there are so many prostate cancer survivors at risk for chronic disabilities and decreased quality of life, reduction of complications and avoidance of adverse outcomes becomes a national health issue. Among the three main treatment options for localized prostate therapy, prostate brachytherapy has emerged as an excellent alternative for patients who meet specific criteria because it offers the benefits of a higher gland specific dose of radiation therapy without the side effects of external beam therapy [4]. The procedure is completed in one session either on an outpatient basis, or requiring an overnight hospital stay. There is no significant blood loss, making this an attractive alternative to surgery. Recent studies have indicated a disease specific survival equal to prostatectomy [5, 6]. All of these factors point to a potential for equal survival with lower morbidity than surgical excision or external beam therapy. For prostate brachytherapy, the success rate of the procedure is directly related to the clinician's level of experience. Therefore, improvements in brachytherapy complication rates will be dependent on improving the tools clinicians use for training to improve the accuracy of needle guidance and deployment of 'seeds' within the prostate gland.

From the surgical simulation viewpoint, most tissue response modeling efforts in the literature are targeted towards assuming mechanical properties and developing methods to efficiently solve the tissue simulation problem for robot-assisted surgery/training. Several simulations have developed very sophisticated virtual environments that allow for plastic deformations of the material and interactions in multiple dimensions [7, 8]. However, it has been difficult to populate these models with data from real tissues. Simulation and modeling of needle insertions have been conducted by a number of researchers [9-18]. However, most assume linear elastic properties, homogenous tissues, and no needle

deflection. Only a few groups have modeled and studied the measurement of forces during needle insertion into soft tissue and the effects of needle geometry on the deflection during needle insertions into homogenous tissues [14, 19]. Needle deflection is an important part of our study because it has been observed during surgical procedures of prostate brachytherapy that the needle can deflect from the initial insertion point as it is being inserted through the body by more than 10mm [20].

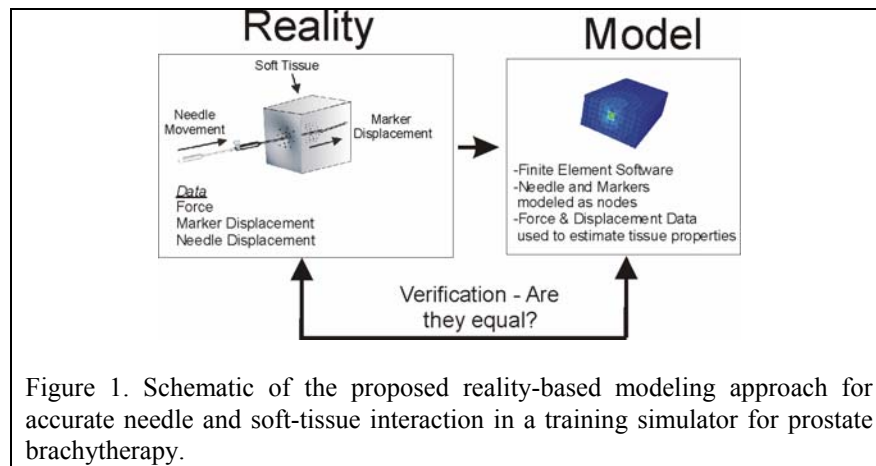


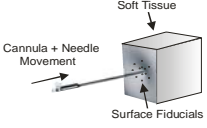
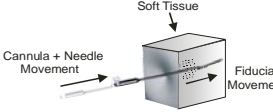
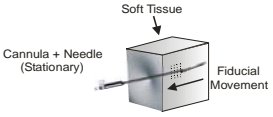
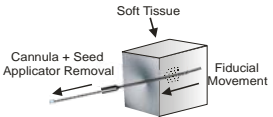
Figure 1. Schematic of the proposed reality-based modeling approach for accurate needle and soft-tissue interaction in a training simulator for prostate brachytherapy.

To the author's knowledge, there has been no work on measuring in real time the 3-D movement of fiducials (beads) in non-homogeneous soft tissue during needle insertion. Our method of tracking beads using two C-ARMS facilitates the extraction of necessary parameters for accurate estimation of needle and soft tissue interaction. *This type of reality based modeling is critical for providing accurate haptic feedback in surgical simulation.* The findings in this study will be used to further the development of an accurate haptic feedback simulator for prostate brachytherapy training. Figure 1 shows a schematic of the proposed reality-based modeling approach.

II. MATERIALS AND METHODS

Table 1 demonstrates our proposed approach for modeling needle and soft-tissue interaction during a needle insertion and withdrawal task in prostate brachytherapy. Each task is broken down into the experimental tools needed, data acquired during the experiment and computational tools used for analysis. This paper presents: a) the computation model for task 1 to estimate the local tissue stiffness prior to puncture and b)

reality-based estimation of needle and soft tissue interaction for tasks 2 and 3.

Table 1. Modeling needle and soft-tissue interaction during needle insertion and withdrawal		
Tasks	Tools	Data Acquired
<p>1. Needle Puncture</p> 	<p>Exp. Tools</p> <ul style="list-style-type: none"> -External Vision Sys. -JR3 -Fiducials on perineum -DSpace 1103 <p>Comp. Tools</p> <ul style="list-style-type: none"> -ABAQUS -MATLAB 	<ul style="list-style-type: none"> -Fiducial movement on skin surface -Force vs. displacement prior to skin puncture
<p>2. Soft-tissue and needle interaction (needle insertion)</p> 	<p>Exp. Tools</p> <ul style="list-style-type: none"> -2 C-ARMS -JR3 -Fiducials inside tissue -DSpace 1103 <p>Comp. Tools</p> <ul style="list-style-type: none"> -ABAQUS -MATLAB 	<ul style="list-style-type: none"> -Force vs. displacement -Fiducial movement -Local tissue motion -Global tissue movement
<p>3. Tissue relaxation</p> 	<p>Exp. Tools</p> <ul style="list-style-type: none"> -2 C-ARMS -JR3 -Fiducials inside tissue -DSpace 1103 <p>Comp. Tools</p> <ul style="list-style-type: none"> -ABAQUS -MATLAB 	<ul style="list-style-type: none"> -Force decay over time -Fiducial movement -Local tissue movement -Global tissue movement
<p>4. Cannula + Seed applicator removal</p> <ul style="list-style-type: none"> -Seed recoil -Cannula-tissue friction force 	<p>Exp. Tools</p> <ul style="list-style-type: none"> -2 C-ARMS -JR3 -Fiducials inside tissue -Seed insert -DSpace 1103 <p>Comp. Tools</p> <ul style="list-style-type: none"> -ABAQUS -MATLAB 	<ul style="list-style-type: none"> -Force vs. disp. -Fiducial / seed movement -Local fiducial movement vs. relaxed state -Global tissue movement -Cannula and needle friction force

Needle insertion device: The needle apparatus was designed to measure the forces on a surgical needle during insertion into soft tissue. The insertion and withdrawal speeds varied from 1.14 mm/sec to 25.4 mm/s. The needle insertion device consisted of a geared DC motor, an incremental encoder and a JR3 precision 6 axis force/torque sensor. The JR3 sampled the force at 1000 Hz. For our experiments, we used an 18-gauge prostate seeding needle (Mick Radio Nuclear Instruments, Inc.) of length 20 cm. This is consistent with the type of needle typically used by surgeons when performing prostate brachytherapy (Figure 2).

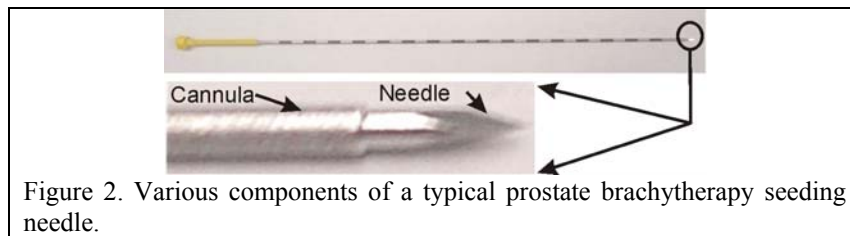


Figure 2. Various components of a typical prostate brachytherapy seeding needle.

Soft Tissue Markers: To view the internal tissue movement during needle insertion, forty 1mm diameter stainless steel beads were inserted into the soft tissue. These beads were chosen because their size was small enough to not affect the properties of the soft tissue or impede the needle insertion path. They also show up well under X-ray imaging. The beads are placed in a grid pattern spaced approximately 5mm apart from one another. The grid was meticulously placed to avoid occlusion between beads during imaging. Each bead was inserted perpendicular to the experiment needle path using an 18 gauge needle to an approximate depth of 10 to 20 mm from the tissue surface.

Dual C-arm Fluoroscopes for bead tracking: Two C-ARM Fluoroscopes were used to image the fiducial markers and the needle during insertion. C-ARM Fluoroscopy allows for real time X-ray imaging where X-rays are generated at the transmitter and photographed at the receiver. The C-ARMS were positioned so that their imaging planes were orthogonal to each other, allowing for real time imaging of the side and top views of the soft tissue fiducial markers and needle during insertion (Figure 3a). The video images of each C-ARM were captured onto a hard disk using a video capture device (Pinnacle Systems) at 30 frames per second at a resolution of 720 x 480 pixels.

Marker Registration: Once the soft tissue was in place for the experiment, a 1mm graduation radiopaque ruler (Lightek Corporation) was imaged in side view and top view to obtain the conversion for image length in pixels to length in millimeters. Using the two C-ARM configuration, we were able to correlate the beads in the top view with the beads in the side view because of the C-ARM ability to continually image as it is rotated from 90 to 180 degrees. Each bead could then be tracked as it moved in the image from the top view to the side view. This was done before inserting the needle for each soft tissue sample.

After bead registration, the needle was moved into place and inserted approximately 90 mm into the soft tissue at three different speeds, namely: 1.14, 12.7, and 25.4 mm/s. During the insertion, the JR3 force sensor captured the forces acting on the needle while the side view C-ARM and top view C-ARM continually recorded X-ray images of the needle position and the movement of beads inside the tissue (Figure 3b).

After each insertion, the needle was moved to a different position in the soft tissue to minimize the chance of following a previous insertion path.

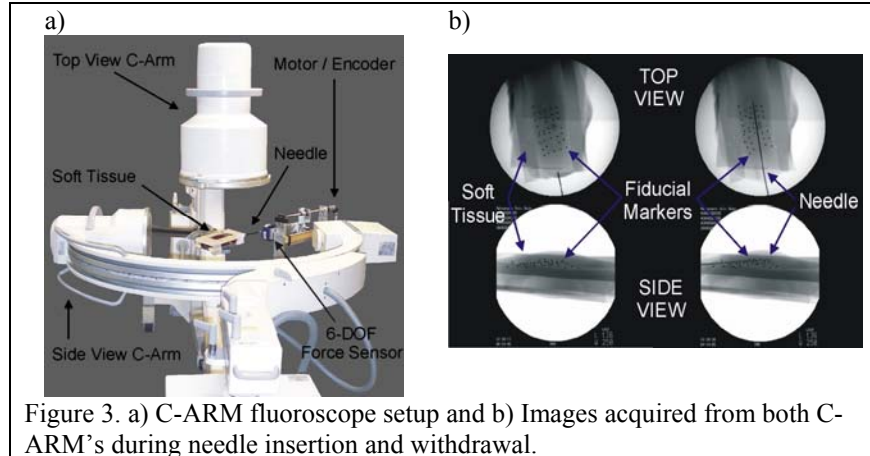


Figure 3. a) C-ARM fluoroscope setup and b) Images acquired from both C-ARM's during needle insertion and withdrawal.

MATLAB image processing toolbox combined with standard kinematic transformations was used to extract the bead and needle coordinates in the global frame from the top and side view X-ray images. The videos from the top and side views for each insertion were loaded separately into MATLAB as .avi files. An image difference algorithm was then applied from an image of the soft tissue with no beads to the frame being analyzed. The new difference image highlighted the bead and needle movement between the frames.

III. RESULTS AND DISCUSSION

A. Needle-Soft tissue interaction forces

Based on needle and soft-tissue interaction during puncture events, the three graphs in Figure 4a represent insertion of the needle into 3 different soft tissue samples. Needle insertion consists of 4 events as shown in Table 1, namely: puncture, insertion, relaxation, and withdrawal. The forces acting on the needle are: the force at the tip of the needle required for cutting the tissue, the friction force of the tissue sliding along the needle shaft, and the clamping force of the tissue on the needle [14]. As the needle inserts farther into the soft tissue, it undergoes a series of micro punctures where the force rises a small amount and then drops down. Once the needle is inside the tissue, the force increases relatively linearly; with the exception of a few major puncture events along its path resulting from significant change in tissue stiffness due to its non-homogeneity. A puncture event comprises of initial deformation

(leading to a rise in the force reading in the force sensor) followed by puncture (sudden drop in the force reading). The force increases linearly during insertion due to the increased surface area of the needle inside the tissue (friction force along the cannula length) and clamping force of the tissue around the needle. Based on our experimental observations, we hypothesize that in a typical puncture event the tissue is deformed at the same rate as the velocity of the needle tip. This causes a quick increase in force until puncture occurs. Based on this rationale, Figure 4b illustrates ten major puncture events for a sample of soft tissue.

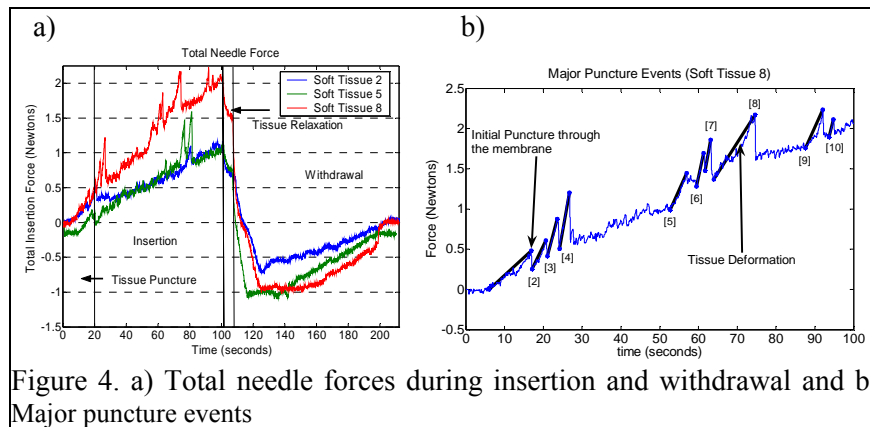


Figure 4. a) Total needle forces during insertion and withdrawal and b) Major puncture events

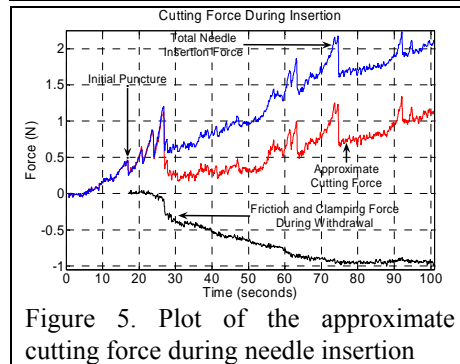


Figure 5. Plot of the approximate cutting force during needle insertion

We found that separating the cutting tip force from the friction force on the needle is a challenging experimental task. Our approach for estimating the needle-tissue interaction force purely due to cutting was to subtract the force data during the withdrawal portion of the experiment from the force data

during the insertion part of the experiment. Figure 5 shows the approximate cutting force based on this approach.

B. Estimating needle trajectory, bead movement, and tissue relaxation

Figure 6 shows the trajectory of the needle through the soft tissue during insertion and withdrawal. Deflection of the needle tip from the straight line trajectory was observed during the experiment. Needle deflection is important to measure and predict for training radiation oncologists to place seeds accurately in the prostate. In a typical prostate

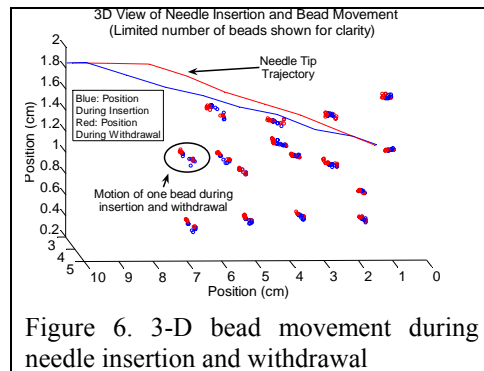


Figure 6. 3-D bead movement during needle insertion and withdrawal

brachytherapy task the needle can deflect as much as 10 mm from the initial insertion point [20] which requires recomputation of the dosage information for radioactive seed placement. In our studies, the needle was shown during some insertions to deflect approximately 9.75 mm away from the straight line trajectory. Most of the

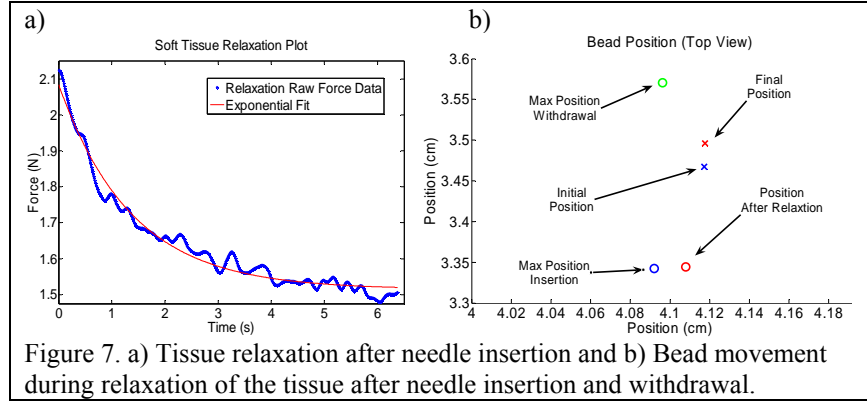
deflection was caused during the initial puncture due to the force produced by tissue deformation although deflection was also caused by the inhomogeneity of the soft tissue, generating asymmetric forces on the needle.

Figure 6 also illustrates the movement of the beads during a typical needle insertion and withdrawal in soft tissue. Each cluster in Figure 6 represents the area covered by the movement of a bead with the surrounding tissue. For clarity, we have only shown a small subset of beads actually used in the experiment. The needle was inserted at 12.7 mm/sec to a depth of approximately 9.5 cm. Each bead has a corresponding blue color for its position during insertion and red color for its position during withdrawal. Beads closest to the needle path showed the largest range of movement while the movement of beads farther away from the needle path was less. The estimated movement of the beads is used to validate a finite element model to predict soft tissue deformation during needle insertion and withdrawal task.

Tissue relaxation is a very important parameter to understand when simulating seed placement for prostate brachytherapy. Relaxation can cause a seed to be placed in an inaccurate location. Tissue relaxation can be observed by analyzing the force data as the needle is held in its full insertion position. Figure 7a illustrates the relaxation of the tissue occurring based on the force data. Figure 7b represents the top view of the tissue sample for the movement of one bead inside the tissue close to the needle path during both needle insertion and withdrawal task. Both needle insertion and withdrawal contribute to tissue relaxation, namely relaxation after the needle reaches its final position in the tissue and relaxation after the needle is completely withdrawn from the tissue. Tissue relaxation based on movement can be seen from the difference in the position of the bead after full insertion and the position of the bead after tissue relaxation has occurred while holding the needle in place.

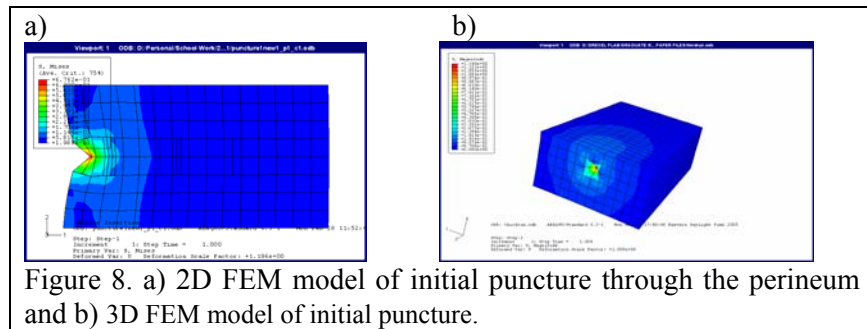
Based on our experimental data, we can initially model the tissue relaxation process at the end of an insertion task as an exponentially decaying curve given by:

$$y = 0.5689e^{-0.7276x} + 1.5149 \quad (1)$$



C. Modeling Needle Puncture

Based on our experimental data, we have recently modeled step 1 of Table 1, namely tissue puncture. A plane stress finite element model, using 4 node quadrilateral elements was built using the ABAQUS software (Version 6.3) as shown in Figure 8a. Figure 8b shows a 3D model of tissue deformation prior to puncture.



We conducted a linear elastic FEM analysis with a Poisson's ratio of 0.3 and an initial local effective modulus of arbitrary magnitude E_1 . The tip of the needle was modeled as a node located at points corresponding to the position of the puncture events shown in Figure 6. For each event, the node was given an experimentally measured displacement ΔU^{EXP} . The computed ΔF^{FEM} from the displacement at that node was compared with the ΔF^{EXP} measured experimentally. Using the initial effective

modulus E_1 , we performed iterations to obtain the ΔF^{FEM} equal to ΔF^{EXP} . The final E value determined is the local effect modulus, $E^{\text{effective}}$, of the tissue during the puncture event (see Table 2). Figure 9 illustrates this computation procedure.

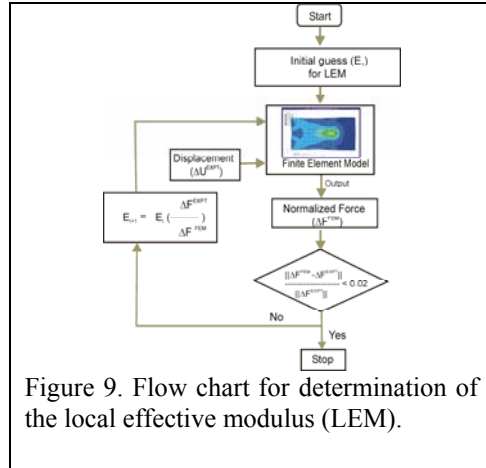


Figure 9. Flow chart for determination of the local effective modulus (LEM).

movement and forces under needle insertion and will be verified with that of experimental data. Figure 8b is an initial three dimensional model with a global mesh of $0.5 \times 0.5 \times 0.5 \text{ cm}^3$, 8-node, solid linear brick element with incompatible modes. Nodes of elements closest to fiducial marker locations are placed at the coordinates of the fiducial markers. The tip of the needle was modeled as a node similar to that of the two dimensional model.

The 3D FEM model has been developed and will also be used to predict soft tissue

Local Effective Modulus During Puncture Events	
Puncture Event	LEM*10 ³ N/m ²
Initial Puncture	9.575
[2]	13.975
[3]	23.833
[4]	34.263
[5]	11.798
[6]	23.325
[7]	30.459
[8]	8.291
[9]	11.541
[10]	21.422

TABLE 2. Local Effective Modulus of Puncture Events

IV. CONCLUSION AND FUTURE WORK

This study demonstrates a unique approach for estimating needle and soft tissue interaction for the simulation of accurate seed placement in prostate brachytherapy. We have shown through the use of 2 C-ARM Fluoroscopes that we can obtain in real time 3D needle trajectory and internal global and local tissue deformation during needle insertion into soft tissue. From this we can extract important parameters for modeling tissue puncture and tissue relaxation. The internal tissue movement can also be used to verify predictions of soft tissue finite element models. Also, we have shown by using the force and displacement data from puncture events that we can quantify the local resistance of the soft tissue to puncture, through the computation of the LEM. Additionally, by subtracting the friction and clamping force during needle withdrawal

from the total needle force during insertion, we can obtain the tissue cutting force during needle insertion.

We propose to develop a three dimensional finite element model for simulating the needle insertion and withdrawal task in prostate brachytherapy. Based on 3D fiducial movement estimated from our current work, we can compute the “strain field” for each fiducial in the image and determine the local effective modulus of the tissue during a needle insertion and withdrawal task.

The work presented in this paper is to our knowledge the first of its kind for modeling needle deflection and soft tissue movement during needle insertion and withdrawal task in prostate brachytherapy. This work will be the basis for developing a reality-based training simulator for training radiation oncologists in prostate brachytherapy.

ACKNOWLEDGEMENTS

We would like to thank Dr. Waqus Anjum and Sajeel Shiromani for their valuable help in conducting dual C-ARM experiments.

REFERENCES

- [1] A. Jemal, "Cancer statistics,," *CA Cancer J.Clin*, vol. 54, pp. 8-29, 2004.
- [2] J. D. Hall, "Why patients choose prostatectomy or brachytherapy for localized prostate cancer: results of a descriptive survey,," *Urology*, vol. 61, pp. 402-407, 2003.
- [3] B. Leak, "Relevant patient and tumor considerations for early prostate cancer treatment,," *Semin.Urol.Oncol.*, vol. 20, pp. 39-44, 2002.
- [4] L. Potters, "Permanent prostate brachytherapy in men with clinically localised prostate cancer,," *Clinical Oncology*, vol. 15, pp. 301-315, 2003.
- [5] J. Sharkey, "Minimally invasive treatment for localized adenocarcinoma of the prostate: review of 1048 patients treated with ultrasound-guided palladium-103 brachytherapy,," *Journal of Endourology*, vol. 14, pp. 343-350, 2000.
- [6] S. E. Langley and R. W. Laing, "Iodine seed prostate brachytherapy: an alternative first-line choice for early prostate cancer,," *Prostate Cancer Prostatic.Dis.*, vol. 7, pp. 201-207, 2004.
- [7] G. Picinbono, H. Delingette, and N. Ayache, "Nonlinear and anisotropic elastic soft tissue models for medical simulation,," presented at IEEE International Conference on Robotics and Automation, vol. 2, pp. 1370-1375, 2001.
- [8] C. Forest, H. Delingette, and N. Ayache, "Cutting Simulation of Manifold Volumetric Meshes,," *Proceedings of the Fifth International Conference on Medical Image Computing and Computer Assisted Intervention*, vol. 2, pp. 235-244, 2002.

- [9] S. P. DiMaio and S. Salcudean, "Needle insertion modeling and simulation," presented at IEEE International Conference on Robotics and Automation, vol. 2, pp. 2098-2105 2002.
- [10] H. Nienhuys and F. van der Stappen, "Interactive needle insertions in 3D nonlinear material," Technical Report UU-CS-2003-019, 2003.
- [11] P. N. Brett, A. J. Harrison, and T. A. Thomas, "Schemes for the Identification of Tissue Types and Boundaries at the Tool Point for Surgical Needles," *IEEE Transactions on Information Technology in Biomedicine*, pp. 30-36, 2000.
- [12] J. Magill, B. Anderson, G. Anderson, P. Hess, and S. Pratt, "Multi-Axis Mechanical Simulator for Epidural Needle Insertion," presented at International Symposium on Medical Simulation, 2004.
- [13] R. Alterovitz, R. Pouliot, R. Taschereau, I. Hsu, and K. Goldberg, "Simulating Needle Insertion and Radioactive Seed Implantation for Prostate Brachytherapy," presented at Medicine Meets Virtual Reality 11, 2003.
- [14] H. Kataoka, T. Washio, K. Chinzei, K. Mizuhara, C. Simone, and A. Okamura, "Measurement of Tip and Friction Force Acting on a Needle During Penetration," *Proceedings of the Fifth International Conference on Medical Image Computing and Computer Assisted Intervention*, pp. 216-223, 2002.
- [15] C. Simone and A. Okamura, "Modeling of Needle Insertion Forces for Robot-Assisted Percutaneous Therapy," presented at IEEE International Conference on Robotics and Automation, vol. 2, pp. 2085-2091, 2002.
- [16] D. Stoianovici, L. Whitcomb, J. Anderson, R. Taylor, and L. Kavoussi, "A Modular Surgical Robotic System for Image Guided Percutaneous Procedures," presented at MICCAI, 1998.
- [17] W. L. Smith, K. Surry, G. Mills, D. Downy, and A. Fenster, "Three Dimensional Ultrasound-Guided Core Needle Breast Biopsy," *Ultrasound in Medicine and Biology*, vol. 27, pp. 1025-1034, 2001.
- [18] J. Hong, T. Dohi, M. Hashizume, K. Konishi, and N. Hata, "An Ultrasound-driven needle-insertion robot for percutaneous cholecystomy," *Physics in Medicine and Biology*, vol. 49, pp. 441-455, 2004.
- [19] M. D. O'Leary, C. Simone, T. Washio, K. Yoshinaka, and A. M. Okamura, "Robotic Needle Insertion: Effects of Friction and Needle Geometry," *IEEE International Conference on Robotics and Automation*, vol. 2, pp. 1774-1780, 2003.
- [20] R. A. Cormack, C. M. Tempany, and A. V. D'Amico, "Optimizing Target Coverage by Dosimetric Feedback During Prostate Brachytherapy," *International Journal of Radiation Oncology Biology and Physics*, vol. 48, pp. 1245-1249, 2000.